Digest Journal of Nanomaterials and Biostructures Vol. 14, No. 3, July - September 2019, p. 617 - 625

# ANNEALING TEMPERATURE EFFECT ON STRUCTURAL, OPTICAL AND PHOTOCATALYTIC ACTIVITY OF NANOCRYSTALLINE $TiO_2$ FILMS PREPARED BY SOL-GEL METHOD USED FOR SOLAR CELL APPLICATION

S. M. AL-SHOMAR[a,*], W. R. ALAHMAD[b]
[a]*Physics Department, Faculty of Science, Hail University, Hail, Saudi Arabia*
[b]*Chemistry Department, Faculty of Science, Hail University, P. O. Box 2440, 81451 Hail, Saudi Arabia*

$TiO_2$ nanocrystalline films were successfully deposited onto glass substrates by sol-gel method at different annealing temperatures (0, 300,400,500 and 600$^o$C). The effect of annealing process on structural, optical and photocatalytic Activity were mainly investigated. The structural analysis shows that the un-annealed and films annealed at 300$^o$C are amorphous, and after annealing from 400 $^o$C to 600 $^o$C results in polycrystalline $TiO_2$ thin films. XRD showed the structural orientation of the films especially in (101) plane corresponding anatasa phase of $TiO_2$.Crystallite size and films thickness increase gradually with annealing temperature due to the decrease in concentration of lattice imperfections and enhancement of nucleation and coalescence. $TiO_2$ have highly transmittance in the visible range and the optical band gap value of the $TiO_2$ thin films decreases from 3.95 to 3.65 eV with the annealing temperature increment as a result of the improved crystalline structure. The refractive index as a function of wavelength was determined. The photocatalytic activity of $TiO_2$ shows that the degradation under sun light was high comparing to UV. Thus, the annealing effects on the physical properties of $TiO_2$ thin films will be useful for the formation of highly crystalline and high-transmittance $TiO_2$ thin films for solar cell application.

(Received January 26, 2019; Accepted July 27, 2019)

*Keyword:* Annealing, Thin film, Photo activity, Sol-Gel. $TiO_2$, Nanocrystalline

## 1. Introduction

Recently, the transition metal oxides have constituted a very interesting class of materials because of the various practical applications due to the broad potential to modify their structural, catalytic and optical properties. Among these metal oxides, $TiO_2$ appears as a useful candidate as it offers a promising entry for many applications, such as solar energy conversion, purify polluted water, textiles, paints, cosmetics, gas sensors and self-cleaning [1] due to its high photocatalytic activity, high stability and wide band gap (3.2 eV) [2].

Generally, titanium dioxide has three structural phase; anatase (tetragonal), rutile (tetragonal) and brookite (orthorhombic). Rutile is the stable high temperature phase as a bulk material (generally in the 600–1855°C), but most common application used only anatase phase [3].

It is known that the physical properties of $TiO_2$ material is highly dependent on the method of synthesis and annealing temperature which influences the transformation of polycrystalline $TiO_2$ thin films from amorphous to anatase and followed by rutile phase (Mathews et al. [4-6]

Diverse techniques have been employed to fabricate $TiO_2$ thin film including RF sputtering, thermal oxidation, anodic oxidation, spray pyrolysis, reactive sputtering, pulsed laser deposition (PLD) and sol–gel method [5- 7]. Most of these techniques are either not feasible or too expensive for industrial applications.

Among them, the sol–gel method yields stable, adherent, uniform and hard films with good electrical and optical properties. However, some factors that affect the quality of the TiO2 thin films deposited using the sol-gel method include (sol concentration, sol agent, pre-heating temperature, post-annealing temperature and sol aging temperature).

*Corresponding author: shereen-m@hotmail.com

Annealing process is one of the most important factors that can strongly affect the properties of TiO2 thin films. [8] have studied the effect of annealing temperature on TiO2 films prepared chemical bath deposition technique. They found that increase in crystalline size with annealing temperature and improvement in optical and photocatalytic activity of the $TiO_2$ films.

In this paper, $TiO_2$ thin films were prepared on a glass substrate by using the cost effective sol–gel technique. The effects of annealing process on the structural, optical, and photocatalytic activity were investigated for solar cell application.

## 2. Material and method

### 2.1. Material

Titanium (IV) isopropoxide ($Ti(OC_3H_7)_4$) [98%], Methanol, Acetonitrile, Ethanol, Acetic acid ($CH_3COOH$), Acetone and Isopropanol all HPLC grade, were purchased from Sigma-Aldrich. Methylene Blue (MB) from Sigma-Aldrich.

Spin coting (A Chemat technology spin coater KW-4A).

UV-Vis double-beam spectrophotometer (Model UVD-2950), UV source; 50 W xenon lamp (Electro-Technic Products, USA).

Sunlight; Solar irradiance directly (south-west 22.5° from the south) in September and October is 6.35- 5.00 kWh/$m^2$/day onto a horizontal surface.

### 2.2. Synthesis of thin films

The solution prepared by dissolving 1.6 ml Titanium (IV) isopropoxide with 4.65 ml of isopropanol. Then stirred at 60ºC for 10 min., followed by dropwise adding of 5.15 ml of acetic acid ($CH_3COOH$) and stirred for 15 min. finally 12 ml methanol added and stirred for 2 hours to yield a clear homogeneous solution.

The glass substrate cleaned with acetone, ethanol and distilled water. Film deposition carried out in air at room temperature. The spin coating process included two steps. Firstly, at 10 seconds, the spin coating speed was 500 rpm, during which the sol covered the substrate. Secondly, at 30 seconds, the spin coating speed was 3000 rpm; it is important to mention that no more sol was added in this step. Then the film dried in a furnace at 100ºC for 30 min. Finally, to crystalline the films, samples annealed at different annealing temperatures (300, 400, 500, and 600 ℃) in air at a heating rate of

1.65 ℃/ min and cooled down to room temperature.

### 2.3. Characterization of materials

#### *2.3.1. X-Ray analysis*

An X-ray diffractometer with CuKα radiation (λ=1.5406Å) was used to characterize the film structure and to estimate the crystallite size of the particles which annealed at various annealing temperatures.

#### *2.3.2. Thickness measurements*

Thin-film thickness of the samples was measured by the weight method and confirmed by the mechanical stylus method (MSM). The measurements were carried out at the room temperature.

#### *2.3.3. Photo catalytic activity evaluation; MB photo degradation*

The photo catalytic performance of the $TiO_2$ thin films estimated by measuring methylene blue (MB) degradation; MB used as a model contaminant.

The degradation is measured by a UV-Vis double-beam spectrophotometer at an incident wavelength of 665 nm. MB solution; 100 ml deionized water spiked with 2.5 ml (200 ppm) 5 ppm concentration added, 180 min run time, at every 30 min 5 mL sample taken, centrifuged (4000 rpm, 3 min) then analyzed on UV spectrophotometer.

## 3. Results and discussion

### 3.1. Structural characterization

The crystal structure and orientation of the $TiO_2$ thin films were investigated using an X-ray diffractometer in the range 10-80° of diffraction angles, $2\theta$. Fig. 1 shows the XRD patterns of the sol–gel synthesized $TiO_2$ thin films after annealing under various temperatures (un-annealed, 300,400, 500, and 600 °C).

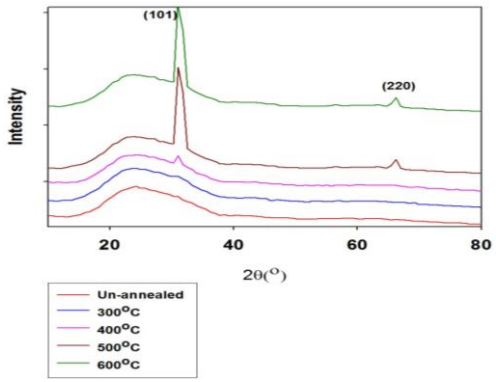


*Fig. 1. X-Ray patterns of un-annealed $TiO_2$ thin films at different annealing temperatures (a) un-annealed (b) 300℃ (c) 400℃ (d) 500℃ and (e) 600℃.*

It is clear from the figure that the au-annealed film and annealed at 300 ºC were amorphous. The (101) anatase peak appeared at the annealing temperature of 400°C and the crystallinity further increased with increasing annealing temperature. A similar result was observed by Lin et al. (2013) [9] when they investigated the effect of annealing temperature on the Photocatalytic Activity of $TiO_2$ thin films coated on soda-lime-silica glass substrates. This characteristic is due to the fact that with increased annealing temperature, the surface mobility increases, the preferred orientation is enhanced, and the adhesion between the particles and the substrate is improved. At 500 ℃ the peak (220) was appeared and sharp increase for the (101) plane is observed compared with others patterns. The position of the observed peaks were found at the following diffraction angles $2\theta = 31.34^{o}$, $65.92^{o}$ corresponding to the Miller indices (101) and (220). The figures show that with increased the annealing temperature to 600°C, the position of (101) peaks shift to higher angles might have been caused due to stress changing in the film.

From Table 1 the full width at half maximum (FWHM) of the (101) diffraction peak decreases with annealing temperature increment. The smallest (FWHM) value is obtained for the films annealed at 600 ºC, which corresponds with the increase in crystallite size and crystalline quality.

The crystallite size $D$ (Eq. 1) of the $TiO_2$ films was estimated from the XRD pattern according to the Debye-Scherrer's relation [10], shown in Table 1:

$$D = \frac{k\lambda}{\beta \cos\theta} \tag{1}$$

where $\lambda$ = X-ray wavelength (1.54184 Å), θ is the Bragg diffraction angle of the XRD peak, and $\beta$ is the FWHM. It was found that the crystallite size increase with annealing temperature increment from 300 ℃ to 600℃. This result can be explained by two reasons. First by raising the annealing temperature, the atomic mobility increases which improved the ability of atoms to find occupy stable position inside the $TiO_2$ crystals. Second, increasing the annealing temperature rapidly reduces the crystallographic defects.

Using Bragg's diffraction law by ($n\lambda=2d_{(hkl)} \sin.\theta_{(hkl)}$), one can calculate the interplanar distance (d) by knowing the wavelength of the used X-ray source, λ=1.54184 Å and the position of the diffraction line (the diffraction angle 2θ). Comparing between the expected and the experimental d-values which were listed in Table 1 for the samples.

From Table 1 can observe that the theoretical estimations are in good agreement with the results of present work.

The calculated lattice parameters a and c of the $TiO_2$ films at different annealing temperatures are present in Table 1. It was noted that the (a) values decrease with increasing the annealing temperatures. This decreasing could have been due to the effect of the stress, which produced from the coalescence of the grain boundaries that found between the crystallites. Whereas, when the film was initially deposited, it consisted of small crystallites and the distances between them is very large. But, when the sample was annealed, the crystallites begin to coalesce with each other and the grain boundaries approaching from each other and even they gather [11].

The internal microstrain ‹ε› can be evaluated using the relation (Eq. 2) [9]:

$$\langle\varepsilon\rangle = \frac{\beta \cot \theta}{4} \tag{2}$$

where β is full-width at half-maximum of the (101) peak. It is clear that when the annealing temperature is increased the strain decreased considerably. This result can be attributed to the decreasing volume occupied by the atoms arranged due to crystallites agglomeration.

The dislocation density which represents the amount of defect in the film was determined from the formula given below (Eq. 3) [12]:

$$\delta = \frac{1}{D^2} \tag{3}$$

where *D* is the crystallite size of $TiO_2$ thin film. Overall, the dislocation density increases with the annealing temperature increases. It may be due to the decrease in concentration of lattice imperfections and improve the crystallite of the deposited films.

*Table 1. Structure parameter of $TiO_2$ thin films deposited on glass substrate at different annealing temperatures.*

| Sample | FWHM ($^o$) | Crystallite size (nm) | d-value experimental | d-value expected | a (A$^o$) | C (A$^o$) | ‹ε› × $10^{-3}$ | δ × $10^{-2}$ (nm)$^{-2}$ |
|---|---|---|---|---|---|---|---|---|
| **300 $^o$C** | 0.470 | 36 | 2.936 | 2.930 | 4.815 | 3.706 | 19.36 | 0.0771 |
| **400 $^o$C** | 0.240 | 71 | 2.952 | 2.968 | 4.790 | 3.748 | 9.69 | 0.01983 |
| **500 $^o$C** | 0.224 | 75.6 | 2.953 | 2.963 | 4.788 | 3.751 | 9.20 | 0.01749 |
| **600 $^o$C** | 0.106 | 159.8 | 2.970 | 2.960 | 4.476 | 3.801 | 4.35 | 0.00391 |

The films thickness values are shown in Fig. 2. It was observed that increasing annealing temperature from 300 to 600 ºC for $TiO_2$ films resulted in increased film thickness. This can be explained as with increasing annealing temperature, the growth rate increases, which in turn to enhances the film thickness and the crystallite size. It also can be attributed to enhancement of nucleation and coalescence of grains [13].

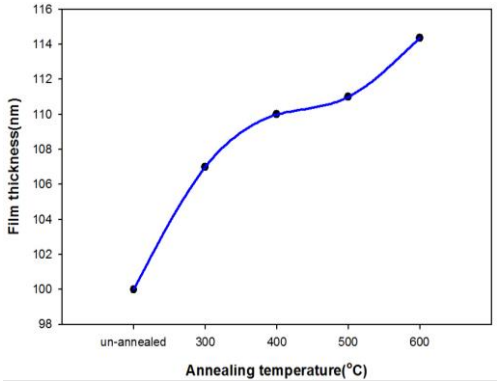


*Fig. 2. The variation of the films thickness of $TiO_2$ thin films with annealing temperatures.*

### 3.2. Optical characterization

Optical transmittance spectra of un-annealed $TiO_2$ thin films and those annealed at different temperatures (300, 400, 500 and 600 ºC) are presented in Fig. 3. It is clear that the au-annealed and annealed $TiO_2$ thin films were highly transparent in the visible range (400 – 700 nm) with a transmittance of approximately 80-90%, which indicates good optical quality. The optical transmittance spectra of the samples gradually decrease in the visible region with increasing annealing temperature from 300 ºC to 600 ºC. This phenomenon may be due to the decrease in optical scattering caused by the reduction in grain boundary density as a result of the increase in crystallites size and film thickness [14].

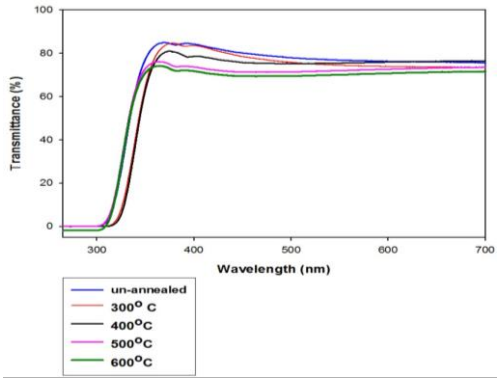


*Fig. 3. Optical Transmission spectra of $TiO_2$ films at different annealing temperatures.*

Fig. 4 shows the UV–Vis absorption spectra of the un-annealed and annealed at various temperature $TiO_2$ thin films. By increasing the annealing temperature from 300 to 600 °C the absorption edge shifts towards the higher wavelength, indicating the decrease in the band gap energy.

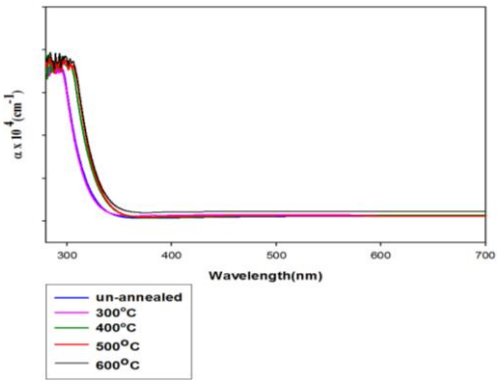


*Fig. 4. Absorbance spectra of $TiO_2$ films at different annealing temperature.*

The annealing temperature also affects others parameters, such as optical band gap ($E_g$). The recombination of electron from the conduction band to the valence band by absorption of photon energy usually occurs either in direct or indirect transitions. The optical band gap of the film can determined by the absorption coefficient using the Eq. 4 [15]:

$$(\alpha h\upsilon) = A(h\upsilon - E_g)^m \tag{4}$$

where $A$ is a constant that depends on the electron-hole mobility with a value between $10^5$ and $10^6$, $\alpha$ is the absorption coefficient ($cm^{-1}$), hν (eV) is the photon energy, and m is equal to ½ for a direct gap and 2 for an indirect gap. Fig. 5 shows the plot between $(\alpha h\nu)^2$ and hν of the un-annealed and annealed films at different annealing temperatures. The extrapolation of linear portion of the curves on (hν) axis gives the direct band gap energy. The spectra shows that the band gap energy of the films (Eg) was decreased from 3.95 to 3.65eV with the increasing of annealing temperature from 300 to 600°C. Annealing led to increased levels of localized near valence band and conduction band and these levels ready to receive electrons and generate tails in the optical energy gap and tails is working toward reducing the energy gap [16]. Also can related to improve the film crystallinity with annealing increment.

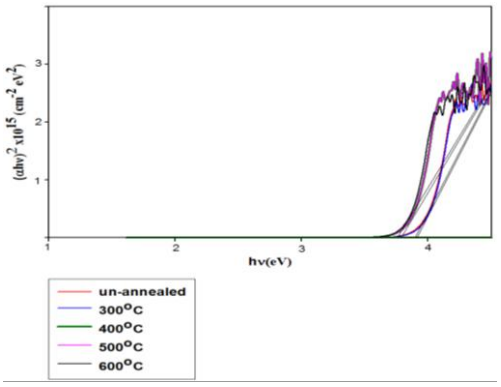


*Fig. 5. Plot of $(\alpha h\nu)^2$ vs hν for $TiO_2$ thin films with different annealing temperatures.*

The refractive index (n) is important properties for an optical material it have been calculated from the Karmers-Kronig equations (Eq. 5-7):

$$R = \frac{(n_1-1)^2 + K^2}{(n_1+1)^2 + K^2} \tag{5}$$

where R is the reflectance and k is the extinction coefficient was calculated using the relation [17]:

$$K = \frac{\alpha\lambda}{4\pi} \tag{6}$$

where α, the absorption coefficient is given by:

$$\alpha = \frac{1}{d}\ln\frac{1-R}{T} \tag{7}$$

where T is the transmittance and d the thickness of the thin film.

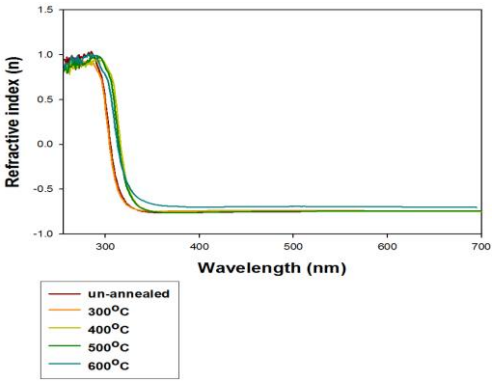


*Fig. 6. The refractive index (n) of $TiO_2$ thin films as a function of wavelength λ at different annealing temperatures.*

From Fig. 6 the *n* values decrease up to certain value with increasing wavelength and these values changes with the annealing temperatures.

It can be seen that, the maximum value of refractive index *n* = 1.08 for un-annealed films at very low wavelength, $\lambda$ = 277 nm (strong-absorption region). The refractive index (n) and decreases with increasing the incident wavelength in the visible range this may be due to changing the film thickness which could change the density and the polarization of the material of the thin films. These results are in good agreement with the data obtained by others [18].

### 3.3. Photo catalytic Activity Evaluation; MB Photo degradation

There are plenty of methods to measure the photocatalytic activity of a material. Some compounds, like methylene blue, methyl orange, methyl red, congo red are used as model compounds to express the photocatalytic activity [19].

The estimation were under UV light and sun light. 50 W xenon lamp (Electro-Technic Products, USA) as a source of UV light. Solar irradiance directly (south-west 22.5$^o$ from the south) in September and October is 6.35- 5.00 kWh/m$^2$/day onto a horizontal surface [20].

Herein MB is used as a model contaminant, the initial and equilibrium dye concentrations were determined using a calibration curve based on absorbance versus dye concentration in the standard dye solutions. To construct a calibration curve; MB concentrations of 0.5, 1.0, 3.0, 5.0, 7.0, 10.0, 15.0, and 20.0 mg/L prepared in volumetric flasks; the absorbance of each of the standard MB solutions measured at the maximum absorption wavelength of 665 nm.

Degradation efficiency Fig 7 below equation (Eq. 8) was used, where Co initial concentration, Ci sample concentration:

$$\textit{Degradation efficiency} = (Co\text{-}Ci/Co)\times 100\% \tag{8}$$

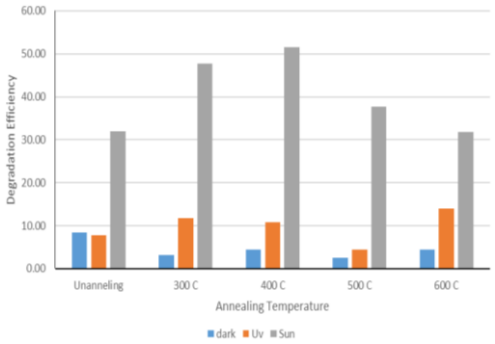


*Fig. 7. Degradation efficiency of thin films at different annealing tempretures under UV light and Sun light.*

The photo activity degradation under sun light was higher comparing to UV light in all films where it ranged between 45-51%.

Photo activity is determined mainly by the photo excitation of ē-h pair, due to light harvesting (which is relevant to band gap) with carriers transfer on surface. Surface properties is greatly affect the processes of photo degradation activity [21-25].

The significant increase in film thickness explain the increase in photo catalytic activity. The effective surface area on the nano-scale may also affect the photo catalytic activities of the films [25].

Herein the thickness of the films ranged from 100-115 nm, which explain the small variation in the photo degradation activity.

## 4. Conclusions

Nanocrystalline $TiO_2$ thin films has been synthesized successfully in room temperature by sol-gel technique using Titanium (IV) isopropoxide as a starting material. The effect of annealing temperature on structural, optical and photocatalytic activity properties are studied. The intensities of the XRD peaks increased with annealing temperature increment and the adhesion between the particles and the substrate is improved. The position of (101) peaks shift to higher angles at annealing temperature 600$^{o}$C. The average crystallite size was found to vary from 36 to 160 nm with increasing in annealing temperatures from (0 to 600$^{o}$C). The optical properties concerning the absorption and transmission spectra were studied for the prepared thin films. The optical band gap were found to be in the range of (3.95 eV to 3.65 eV) and refractive index were change when the film thickness varying from 100 nm to 115 nm. Photo catalytic activity estimated under UV light and sun light using MB a model contaminant, the % degradation of MB ranged from 45-%51%.

### Acknowledgements

The authors would like to thank university of Hail for their device and support.

### Conflict of interest

The author declares that there is no conflict of interest regarding the publication of this paper.

## References

[1] K. M. Muaz, U. Hashim, F. Ibrahim, K. L. Thong, M. S. Mohktar, W. W. Liu, Microsystem Technol. **22**, 871 (2016).

[2] Z. Essalhi, B. Hartiti, A. Lfakir, M. Siadat, P. Thevenin, J. Mater. Environ. Sci. **7**(4), 1328 (2016).
[3] S. K. Shriwastava, S. Singh, IJHIT **9**(2), 267 (2016).
[4] N. R. Mathews, E. R. Morales, M. A. Cortes-Jacome, J. A. Toledo Antonio, Sol Energy **83**, 1499 (2009).
[5] L. Haoa, S. Tang, J. Yanc, L. Chenga, S. Guane, Q. Zhaoa, Z. Zhuc, Y. Luf, Sci. Semicond. Process. **89**, 161 (2019).
[6] M. I. Khan, S. Imran, S. M. Saleem, S. Ur Rehman, Results in Physics **8**, 249 (2018).
[7] C. Natarajan, N. Fukunaga, G. Nogami, Thin Solid Films **322**, 6 (1998).
[8] A. T. Rajamanickam, P. Thirunavukkarasu, K. Dhanakodi, J. Mater. Sci. Mater. Electron. **26**, 8933 (2015).
[9] C.-P. Lin, H. Chen, A. Nakaruk, P. Koshy, C. C. Sorrell, Energy Procedia. **34**, 627 (2013).
[10] P. Scherrer, Gottingen. Mathematisch-Physikalische Klasse. **2,** 98 (1918).
[11] A. A. Akl, S. A. Mahmoud, S. M. AL-Shomar, A. S. Hassanien, Semiconductor Processing (2018).
[12] S. Shanmugan, D. Mutharasu, A. H. Haslan, IJETT **14**(2), 57 (2014).
[13] D. P. Dubal, D. S. Dhawale, A. M. More, C. D. Lokhande, J. Mater. Sci. **46**(7), 2288 (2011).
[14] M. F. Malek, M. H. Mamat, Z. Khusaimi, M. Z. Sahdan, M. Z. Musa, A. R. Zainun, A. B. Suriani, N. D. Md. Sin, S. B. Abd Hamid, M. Rusop, J. Alloys Compd. **582**, 12 (2014).
[15] R. K. Nath, S. S. Nath, K. Sunar, J. Anal. Sci. Technol. **3**(1), 85 (2012).
[16] K. A. Aadim, K. H. Abass, Q. M. Hadi, ILCPA. **56**, 63 (2015).
[17] G. P. Daniel, V. B. Justinvictor, P. B. Nair, K. Joy, P. Koshy, P. V. Thomas, Physica B. **405**, 1782 (2010).
[18] M. M. Abd El-Raheem and Ateyyah M. Al-Baradi, Int. J. Phys. Sci. **8**(31), 1570 (2013).
[19] R. T. Thomas, N. Sandhyarani, RSC Advances. **3**, 14080 (2013).
[20] Solar Irradiance Calculator", Solar Electricity Handbook, 2018. [Online]. Available: http://www.solarelectricityhandbook.com/solar-irradiance.html. [Accessed: 03- Feb- 2018].
[21] Y. Gu, X. Gu, Y. Zhao, Y. Qiang, J. Mater. Sci. (2015). DOI 10.1007/s10854-015-3058-4
[22] G. Fang Huang, Z. Ma, W. Huang, Y. Tian, C. Jiao, Z. Yang, Z. Wan, A. Pan, J. of Nanomaterials (2013). Article ID 371356, 8 pages http://dx.doi.org/10.1155/2013/371356.
[23] C. Tseng, T. Wu, Y. Lin, Materials **11**, 1 (2018).
[24] Y. Penga, Y. Zhanga, F. Tiana, J. Zhanga, J. Yu, Crit. Rev. Solid State 1, (2017).
[25] J. C. Moore, R. Louder, C. V. Thompson, Coatings. **4**, 651 (2014).